Eur. Phys. J. A (2014) **50**: 124
DOI 10.1140/epja/i2014-14124-8

THE EUROPEAN PHYSICAL JOURNAL A

Regular Article – Experimental Physics

Neutron capture cross section measurements for ^{197}Au from 3.5 to 84 keV at GELINA

C. Massimi[1,2], B. Becker[2], E. Dupont[3], S. Kopecky[2], C. Lampoudis[2], R. Massarczyk[4,5], M. Moxon[6], V. Pronyaev[7], P. Schillebeeckx[2,a], I. Sirakov[8], and R. Wynants[2]

[1] Department of Physics, University of Bologna and Sezione INFN of Bologna, Via Irnerio 46, Bologna, 40126, Italy
[2] European Commission, Joint Research Centre - IRMM, Retieseweg 111, B-2440 Geel, Belgium
[3] OECD Nuclear Energy Agency, 12 Bd des Iles, 92130 Issy-les-Moulineaux, France
[4] Helmholtz-Zentrum Dresden-Rossendorf, Postfach 510119, 01314 Dresden, Germany
[5] Technische Universität Dresden, 01062 Dresden, Germany
[6] Hyde Copse 3, Marcham, UK
[7] Institute of Physics and Power Engineering, Obninsk, Russia
[8] Institute for Nuclear Research and Nuclear Energy, Sofia, Bulgaria

Received: 15 April 2014 / Revised: 8 July 2014
Published online: 11 August 2014

Communicated by C. Broggini

Abstract. Cross section measurements have been performed at the time-of-flight facility GELINA to determine the average capture cross section for ^{197}Au in the energy region between 3.5 keV and 84 keV. Prompt γ-rays, originating from neutron-induced capture events, were detected by two C_6D_6 liquid scintillators. The sample was placed at about 13 m distance from the neutron source. The total energy detection principle in combination with the pulse height weighting technique was applied. The energy dependence of the neutron flux was measured with a double Frisch-gridded ionization chamber based on the ^{10}B(n, α) reaction. The data have been normalized to the well-isolated and saturated ^{197}Au resonance at 4.9 eV. Special care was taken to reduce bias effects due to the weighting function, normalization, dead time and background corrections. The total uncertainty due to normalization, neutron flux and weighting function is 1.0%. An additional uncertainty of 0.5% results from the correction for self-shielding and multiple interaction events. Fluctuations due to resonance structures have been studied by complementary measurements at a 30 m flight path station. The results reported in this work deviate systematically by more than 5% from the cross section that is recommended as a reference for astrophysical applications. They are about 2% lower compared to an evaluation of the ^{197}Au(n, γ) cross section, which was based on a least squares fit of experimental data available in the literature prior to this work. The average capture cross section as a function of neutron energy has been parameterized in terms of average resonance parameters. Maxwellian average cross sections at different temperatures have been calculated.

1 Introduction

The neutron capture cross section of ^{197}Au is used as a standard for neutron induced reaction cross section measurements at 0.0253 eV and in the energy range between 200 keV and 2.5 MeV. The use of the ^{197}Au(n, γ) reaction as a reference has several advantages. This is due to the mono-isotopic nature and chemical purity of gold, the relatively large thermal neutron capture cross section and the simple decay scheme of the product nucleus formed by neutron capture.

An evaluation of ^{197}Au(n, γ) reaction cross section data has been reported by Carlson *et al.* [1–3]. This evaluation was a result of an international cooperative effort to improve cross section standards by a Subgroup formed by the Working Party on International Evaluation Cooperation (WPEC) of the Nuclear Energy Agency Nuclear Science Committee and a Coordinated Research Project organized by the International Atomic Energy Agency. The evaluation process was the result of a simultaneous analysis of various types of experimental data: energy dependent, spectrum-averaged and thermal data, including results of ratio and absolute cross section measurements. The evaluation of the ^{197}Au(n, γ) cross section in the energy region between 2.5 keV and 2.5 MeV was based on the results of 62 experiments using a least-squares adjustment code GMA, developed by Poenitz [4]. The full data set, which is given in ref. [2], included results of 21

[a] e-mail: peter.schillebeeckx@ec.europa.eu

absolute ^{197}Au(n,γ) measurements, 6 shape ^{197}Au(n,γ) measurements, 3 absolute ^{197}Au(n,γ)/^{6}Li(n,α) ratio measurements, 3 absolute ^{197}Au(n,γ)/^{10}B(n,α_1) ratio measurements, 3 shape ^{197}Au(n,γ)/^{10}B(n,α_1) ratio measurements, 4 absolute ^{197}Au(n,γ)/^{10}B(n,α) ratio measurements, 9 absolute ^{197}Au(n,γ)/^{238}U(n,γ) ratio measurements, 1 shape ^{197}Au(n,γ)/^{238}U(n,γ) ratio measurement, 10 absolute ^{197}Au(n,γ)/^{235}U(n,f) ratio measurements and 2 shape ^{197}Au(n,γ)/^{235}U(n,f) ratio measurements. In the energy region between 200 keV and 2.5 MeV the result of this evaluation is recommended as a reaction cross section standard with uncertainties between 1% and 4.2%. Between 3.5 keV and 200 keV the uncertainties for the recommended average cross section are between 0.84% and 2.3%. The result of this evaluation will be referred to as the standard evaluation.

Due to strong fluctuations resulting from resonance structures the evaluated cross section below 200 keV is not recommended for use as a standard. Nevertheless, the ^{197}Au(n,γ) cross section in the energy region below 200 keV is used as a reference cross section for astrophysical applications [5]. However, the results of the standard evaluation of refs. [1–3] are approximately 6% to 8% above the cross section adopted for astrophysical applications. The latter is based on the data of Macklin *et al.* [6,7] normalized to the results of activation measurements performed by Ratynski and Käppeler [5]. Results of ^{197}Au(n,γ) measurements from 5 keV to 120 keV reported by Borella *et al.* [8], which were not included in the evaluation process of refs. [1,2], are within 2% consistent with those of the standard evaluation [3]. The cross section recommended in refs. [1,2] are also consistent with the Maxwellian averaged cross section obtained by Feinberg *et al.* [9] and by the time-of-flight data below 30 keV reported by Lederer *et al.* [10]. However, the overall uncertainty of the data in ref. [10] is between 4% and 6.7% and between 30 keV and 100 keV deviations from the evaluated cross section up to 12% are observed.

To clarify the situation capture cross section measurements have been performed at the GELINA facility of the Institute for Reference Materials and Measurements (IRMM) at Geel in Belgium, following the procedures described in ref. [11]. An effort has been made to reduce bias effects due to dead time, background, γ-ray attenuation in the sample, shape of the neutron flux, normalization and corrections for self-shielding and multiple interaction events. An internal normalization procedure based on the well-isolated and saturated 4.9 eV resonance of ^{197}Au [6, 12] was applied and verified by complementary measurements on a thin Au sample. For an accurate determination of the background level, all measurements were performed with fixed background filters. The use of fixed background filters improves the accuracy but results in an upper limit of the data to 84 keV. The accuracy of the correction for self-shielding and multiple interaction events was verified by experiment. To study the impact of resonance fluctuations additional capture measurements on ^{197}Au at a 30 m measurement station were carried out.

2 Experiment

The experiments were carried out at the neutron Time-of-Flight (TOF) facility GELINA. A detailed description of GELINA can be found in ref. [13]. Intense pulsed electron beams are accelerated, at a repetition rate between 50 Hz and 800 Hz, to a maximum energy of 150 MeV. Electron bunches, with peak currents of 12 A in a 10 ns time interval, are compressed by a post-acceleration compression magnet to a duration of less than 1 ns [14]. High-energy electrons generate Bremsstrahlung in a mercury-cooled rotating uranium target, where neutrons are produced by (γ,n) and (γ,f) reactions [15]. To produce a neutron spectrum in the low energy region, two water-filled beryllium containers of 4 cm thickness are used as moderators. BF_3 proportional counters, placed at different locations around the neutron target hall, are used to monitor the stability of the accelerator and to normalize TOF-spectra to the same total neutron intensity.

The measurements were performed at a 13 m measurement station of flight path 5, which forms an angle of 18° with respect to the normal of the moderator face viewing the flight path. A shadow bar made of Cu and Pb was placed close to the uranium target to reduce the intensity of both the γ-ray flash and the fast neutron component. The moderated neutron beam was collimated to about 80 mm in diameter at the sample position. The collimation system was mainly composed of B_4C mixed with epoxy resin, H_3BO_3 mixed with wax, Cu- and Pb-collimators. To minimize the influence of nearby flight paths, shielding walls were built around the detectors. Almost half way between the neutron target and the sample position, *i.e.* just outside the 3 m thick wall of the bunker containing the neutron-producing target, a sample changer for overlap and black resonance filters was installed. The ^{197}Au(n,γ) measurements have been performed with the accelerator operating at 800 Hz and a ^{10}B overlap filter, with an areal density of about 5×10^{-3} at/b. Fixed Na and S black resonance filters were used to continuously monitor the background at 2.85 keV and 102 keV. Due to the presence of the S-filter no additional filter was needed to reduce the intensity of the γ-ray flash. An air-conditioning system was installed in the measurement station to keep the sample at a constant temperature of about 22 °C and to avoid electronic drifts due to temperature changes. In addition, the temperature at the sample position was continuously monitored.

The prompt γ-rays originating from a capture reaction were detected by a pair of C_6D_6-based liquid scintillators (NE230) of 10 cm diameter and 7.5 cm length. Each detector was positioned at an angle of 125° with respect to the direction of the neutron beam. This geometry minimises systematic effects due to the anisotropy in the primary γ-ray emission which depends on the spin and orbital momentum of the resonance. The detection of scattered neutrons was reduced by coupling each scintillator to a boron-free quartz windowed EMI9823-KQB photomultiplier (PMT). For each detector the anode signal from the PMT was used to determine the arrival time of the neutron and the signal of the 9-th dynode to determine

Table 1. Characteristics of the samples used in the capture measurements at GELINA. All samples were in the form of a metal disc.

Sample	Diameter	Thickness	Weight	Area	Areal density
	mm	mm	g	cm^2	at/b
^{197}Au	80.76	1.01	98.7612 ± 0.0002	51.22 ± 0.01	$(5.896 \pm 0.001) \times 10^{-3}$
^{197}Au	80.94	0.52	50.9234 ± 0.0005	51.45 ± 0.01	$(3.026 \pm 0.001) \times 10^{-3}$
^{197}Au	80.12	0.01	0.9483 ± 0.0001	50.39 ± 0.01	$(5.754 \pm 0.001) \times 10^{-5}$
^{208}Pb	80.00	0.50	29.7320 ± 0.0001	50.27 ± 0.01	$(1.713 \pm 0.001) \times 10^{-3}$

the energy deposited by the γ-ray in the detector. The total energy detection principle in combination with the pulse height weighting technique [11,16,17] was applied to make the detection efficiency for a capture event directly proportional to the total γ-ray energy available in the capture event. The discrimination level of the capture detection system was set to 200 keV deposited energy, corresponding to the Compton edge of a 330 keV γ-ray. In the calculation of the weighting function the γ-rays were supposed to be distributed homogeneously in the sample and the discrimination level of the detection system was taken into account, as discussed in ref. [17]. Due to the relatively low total cross section, the homogeneous distribution of γ-rays is valid in the unresolved resonance region. However, this assumption is not valid in the region of a strong resonance like the 4.9 eV resonance of ^{197}Au, which was used for the normalization. To account for the difference in the γ-ray attenuation due to neutron self-shielding, the procedure proposed in refs. [11,18] and implemented in REFIT was applied.

The shape of the neutron spectrum was measured in parallel with a ^{10}B Frisch gridded ionisation chamber placed at about 80 cm before the sample. The chamber was operated with a continuous flow of a mixture of argon (90%) and methane (10%) at atmospheric pressure. The detector consisted of two ionization chambers with a common cathode loaded with two layers of ^{10}B. The ^{10}B layers, with an effective diameter of 84 mm and areal density of about 40 μg/cm^2, were evaporated back to back on a 30 μm thick aluminium backing and the entrance and exit windows of the chamber had a thickness of 40 μm.

The TOF of a neutron was derived from the difference between the stop signal T_S either from the ^{10}B-chamber or from the C_6D_6 detectors and the start signal T_0, given at each electron burst. This time difference $(T_S - T_0)$ was measured with a multi-hit fast time coder with a 0.5 ns resolution, developed at the IRMM [19]. The TOF and the pulse height of the detected events were recorded in list mode using a data acquisition system developed at the IRMM [20], allowing for a continuous stability check of the detection systems and an off-line application of the weighting function. The stability of the two detection systems and the accelerator operating conditions (*i.e.* frequency, current and neutron output) were verified in cycles of 1 hour. Only cycles with a 800 Hz operating frequency and for which the total neutron intensity and response of the detection systems deviated from the average by less than 2.5% were selected. The stability of the C_6D_6 detectors was monitored on a weekly basis by measurements of the 2.6 MeV γ-ray from the ^{232}Th decay chain.

Each detection system produced a veto signal that created a fixed dead-time as soon as an event was detected. The fixed dead time of the capture and neutron detection chains were monitored continuously by registering the time-interval between successive events. For the flux measurements the dead time was 3500 ns, with a maximum dead time correction less than 1%. The dead time for the capture measurement systems was 2800 ns, with dead time corrections that were less than 20%. In refs. [11,21] it was shown that uncertainties for such dead time corrections are very small and can be neglected.

Capture cross section data for ^{197}Au were deduced from results of measurements with a 0.52 mm and 1.01 mm thick metallic gold disc. Additional measurements with a 0.01 mm thick Au metallic disc were performed to verify the normalization. A 0.5 mm thick metallic ^{208}Pb disc was used to determine the sample dependent background contribution in the C_6D_6 response. The main characteristics of these samples, all with a 80 mm nominal diameter, are given in table 1. The areal density was derived from a measurement of the weight and the effective area. The latter was determined by an optical surface inspection with a microscope-based measurement system from Mitutoyo [22].

3 Data reduction

The experimental yield $Y_{\rm exp}$ was deduced from the ratio of the response of the capture detection system and the one of the neutron flux detector [11],

$$Y_{\rm exp} = \frac{N_C}{S_n + E_n \frac{A}{1+A}} \frac{C_w - B_w}{C_\varphi - B_\varphi} \frac{Y_\varphi}{T_\varphi}, \qquad (1)$$

where N_C is a normalization factor, E_n is the kinetic energy of the neutron, S_n is the neutron separation energy and A is the mass number of the target nucleus. The dead-time corrected weighted C_6D_6 response is denoted by C_w and the dead-time corrected response of the flux detector by C_φ. Their corresponding background contributions are B_w and B_φ, respectively. The ratio of the reaction yield of the boron chamber Y_φ and the attenuation of the flux in the chamber T_φ, dependent equivalently on TOF or

energy, is given by

$$\frac{Y_\varphi}{T_\varphi} = e^{n_\varphi \sigma_{\rm tot}}(1 - e^{-n_\varphi \sigma_{\rm tot}})\frac{\sigma_\alpha}{\sigma_{\rm tot}}, \qquad (2)$$

where n_φ is the total areal density of the ^{10}B layers in the ionization chamber, σ_α the cross section for the ^{10}B(n, α) reaction and $\sigma_{\rm tot}$ the total cross section for neutron induced reactions in ^{10}B. Before applying eq. (1) a transformation of variables was applied to account for the 80 cm difference in the position of the ionization chamber and the capture sample. This transformation is required to bring the capture and flux spectrum to the same time basis.

The normalization factor N_C in eq. (1) accounts for energy independent factors such as the absolute neutron flux, the effective target area seen by the neutron beam, the efficiency of the flux detector and the solid angle subtended by the target and the C_6D_6 detectors. This factor was deduced from an internal normalization based on the 4.9 eV saturated resonance of ^{197}Au [6,12].

The impact of kinematic effects for the flux measurements was strongly reduced by using a flux detector consisting of two ionization chambers with a common cathode loaded with two layers of ^{10}B. The back-to-back configuration together reduces a systematic bias related to the forward-to-backward emission ratio [23]. The response C_φ was obtained from a weighted sum of the response of the two chambers. The weights were based on the relative thickness of the layers, which was deduced from a TOF spectrum at low energies obtained from measurements at 50 Hz.

The data processing was carried out using the AGS (Analysis of Geel Spectra) package [24,25]. This package includes all basic spectrum operations and performs a full uncertainty propagation accounting for both correlated and uncorrelated uncertainty components and results in a substantial reduction of space for data storage. The AGS concept is recommended by the Network of Nuclear Reaction Data Centres to store experimental data in the EXFOR data base [26].

3.1 Background correction for flux measurements

The background contribution for the flux measurements was approximated by an analytical expression applying the black resonance technique [11]. The analytical function was a sum of a time-independent and two time-dependent components:

$$B_\varphi(t) = a_0 + a_1 t^{b_1} + a_2 e^{-b_2(t+t_0)}. \qquad (3)$$

The parameters (a_0, a_1, a_2, b_1 and b_2) in the analytical expression were derived from the dips in the TOF-spectra created by black resonances filters. The time independent component a_0 was less than 0.1%. The first time dependent component, approximated by a power function, accounts for neutrons that are scattered inside the detector station and from neutrons scattered at other flight paths. Its time dependence was determined by measurements at

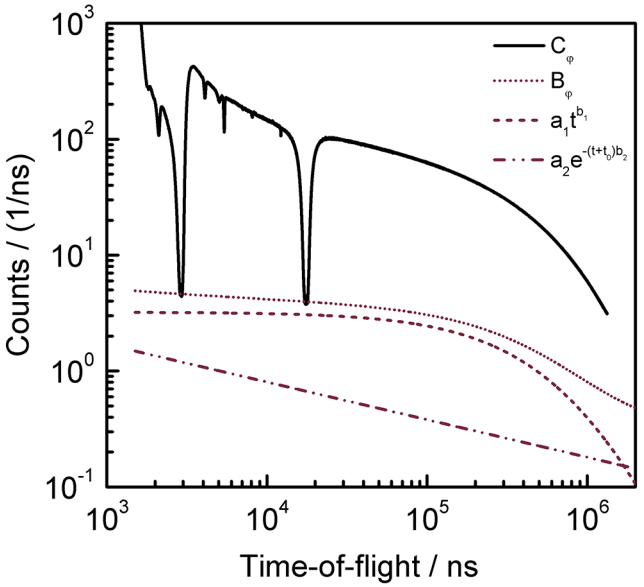

Fig. 1. Time-of-flight spectrum resulting from the flux measurement (C_φ) together with the total background (B_φ) and its time-dependent components due to scattered and overlap neutrons.

400 Hz with a 1 mm thick Cd anti-overlap filter and Ag, W, Co, Na and S black resonance filters. The second time dependent component corresponds to the contribution due to slow neutrons from previous accelerator pulses. This contribution was estimated by an extrapolation of the TOF spectrum at the end of the cycle. It is approximated by an exponential decay, where the fixed time offset t_0 is equal to the spacing between the electron bursts. For an operating frequency of 800 Hz, t_0 = 1.25 ms. For each configuration the amplitudes a_1 and a_2 were adjusted to the black resonance dips at 2.85 keV and 102 keV due to the fixed Na and S filters. The response of the ionization chamber and the estimated background contribution for the ^{197}Au(n, γ) measurements are compared in fig. 1. From a statistical analysis of the difference between the observed black resonance dips and the background estimated by the analytical expression (eq. (3)), an uncertainty of 3% on the determination of the background level was deduced. The uncertainty on the experimental yield $Y_{\rm exp}$ due to the flux background is less than 0.25%.

3.2 Background correction for the C_6D_6 response

The total background contribution to the weighted response of the C_6D_6 detectors was expressed as

$$B_w(t) = b_0 + k_1 C_{w,0}(t) + k_2 R_n(t)[C_{w,{\rm Pb}}(t) - C_{w,0}(t)], \quad (4)$$

where b_0 is a time-independent contribution, $C_{w,0}$ and $C_{w,{\rm Pb}}$ are the weighted counts from measurements with no sample and with an almost purely scattering ^{208}Pb sample, respectively. The weighted spectra $C_{w,0}$ and $C_{w,{\rm Pb}}$, corrected for the time independent background, were derived with the weighting function for the Au sample and

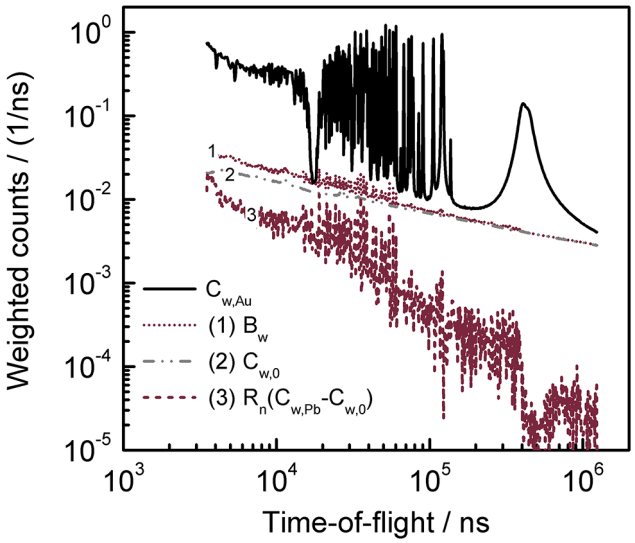

Fig. 2. Weighted time-of-flight spectra obtained with the C_6D_6 detectors. The spectrum for the 1 mm thick Au sample $C_{w,\mathrm{Au}}$ is compared with the total background B_w and the contributions explained in eq. (4) (see text).

normalized to the same integrated neutron intensity. The correction factor R_n is the ratio of the neutron scattering yield of the Au and Pb sample. For energies above 2 keV (TOF-values smaller than 10^4 ns), the corresponding sample-dependent background was less than 2%, as shown in fig. 2. The factors $k_1 = 1.00 \pm 0.03$ and $k_2 = 1.00 \pm 0.05$ were used to introduce uncertainties due to systematic effects in the background model. These values together with their uncertainties were obtained from a comparison of the background based on eq. (4) and the background dips present in the TOF spectra due to the fixed black resonance filters and in the spectra resulting from additional measurements with Ag, Co and Bi black resonance filters. This procedure was carried out for the 0.01 mm, 0.52 mm and 1.01 mm thick Au samples.

3.3 Normalization

The data for the 0.52 mm and 1.01 mm thick Au samples were internally normalized based on the peak of the well-isolated and saturated resonance at 4.9 eV, which has a low scattering to capture ratio. The normalization was obtained by a least squares adjustment of the experimental yield with only the normalization factor as a free-fitting parameter. The REFIT code [27], which is based on the Reich-Moore approximation of the R-Matrix theory, was used. This code accounts for various experimental effects such as the Doppler effect, neutron self-shielding, multiple interaction events, and the response function of the TOF-spectrometer. To account for the impact of the neutron flux and γ-ray attenuation in the sample on the weighting function a special procedure has been implemented in REFIT [11,18]. In this approach the experimental yield is calculated with a weighting function for a homogeneous distribution of the γ-rays in the sample and a correction factor depending on the resonance strength and areal density is applied to the calculated yield. By restricting the fit region to the resonance top, the normalization is independent of the resonance parameters and the areal density, as demonstrated in refs. [8,18].

Table 2. Normalization factors for the capture measurements using the ^{197}Au samples specified in table 1. The factor $N'_{C,51.45}$ corresponding to a sample with an area of 51.45 cm^2 is also given.

Thickness mm	Area cm^2	N_C	$N'_{C,51.45}$
1.01	51.22	0.995	0.991
0.52	51.45	1.000	1.000
0.01	50.39	1.026	1.005

The normalization factors derived from the 4.9 eV saturated resonance in the 0.52 mm and 1.01 mm sample data are given in table 2 and compared with the one derived from the measurements with the 0.01 mm sample. For the 0.01 mm sample the 4.9 eV resonance is not saturated. The normalization for these measurements was obtained from an analysis of the 4.9 eV resonance fixing the resonance parameters to those reported in ref. [28]. These normalization factors depend on the sample area. In the last column, the normalization factors corresponding to a sample with an area of 51.45 cm^2 are also given. These values demonstrate the validity of the weighting function and the procedure to account for the flux and γ-ray attenuation in the sample.

As noted in refs. [8,11,17] the influence of systematic effects depending on the specific character of the γ-ray cascade are largely reduced when the γ-ray emission cascade for the normalization resonance is similar to the cascade for the energy region under investigation. If, in addition, an internal normalization is applied all experimental conditions remain unchanged and bias effects are substantially reduced. To verify the impact of a difference between the prompt γ-ray emission spectrum of the 4.9 eV resonance and the spectrum for the unresolved resonance region, the amplitude spectrum of the 4.9 eV resonance was compared with the one for neutrons with energies between 10 keV and 20 keV and 40 keV and 80 keV. The comparison in fig. 3 reveals a small difference, which is probably due to the increasing contribution of neutrons with $\ell > 0$, and suggests a difference in γ-ray cascade. Therefore, a bias due to a different influence of the 200 keV discrimination level for the 4.9 eV resonance and the neutron energy region above 5 keV cannot be excluded.

To quantify such a bias, the count losses due to the discrimination level were estimated by simulated γ-ray spectra resulting from capture states with different spin, parity and energy. The spectra were simulated using the statistical code γDEX [29,30]. This code follows the basic assumptions made in the DICEBOX code described in ref. [31]. In contrast with the DICEBOX code, the model in γDEX averages over multiple states with same spin and parity and calculates average transition widths between

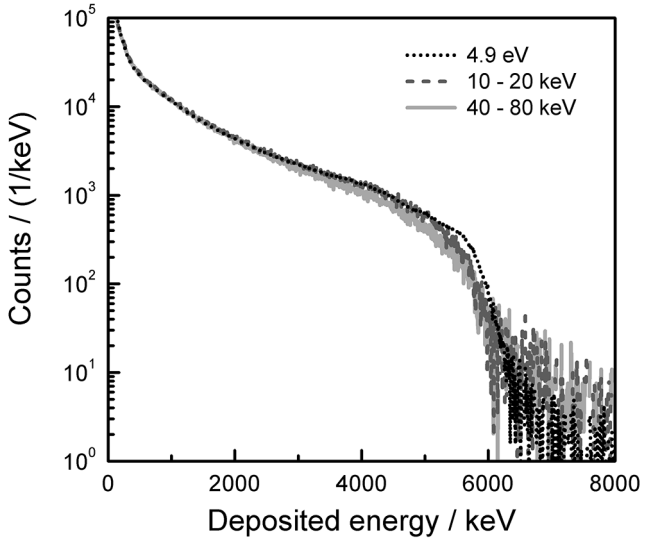

Fig. 3. Response of the C_6D_6 detector, corrected for background contributions, for the 4.9 eV *s*-wave resonance of ^{197}Au and for ^{197}Au(n, γ) events with neutron energies between 10 keV and 20 keV (red) and 40 keV and 80 keV (blue).

energy bins. As long as the number of states within an energy bin is high, such a statistical approach can be applied to simulate γ-ray cascades following primary transitions to the continuum. On the contrary the statistical assumption is not sustained for primary transitions to the ground state and excited states close to the ground state.

For the level density in the continuum, a constant temperature model was assumed with the parameter $kT = 670$ keV and an average resonance spacing $D_0 = 15.69$ eV at zero neutron energy. The $E1$ γ-ray strength was approximated by a triaxial Lorentzian description [32]. For the $M1$ strength a parametrization proposed by Heyde *et al.* [33] that results from an adjustment to experimental data was used. For $E2$ strengths the recommendation of the RIPL3 data base [34] was followed.

In the calculation the characteristics of the first ten excited states of ^{198}Au, *i.e.* their spin and parity as well as their transition strengths and branching ratios, were taken from the ENSDF database [35]. For the 4.9 eV resonance the absolute transition strengths of primary transitions (*i.e.* absolute intensity per capture event) to these low lying states have been determined experimentally and were taken from [35]. Their relative contribution to the total primary emission intensity is about 17%. In the unresolved resonance region (URR) absolute intensities of primary transitions to low-lying excited states are not available. For 2 keV and 24 keV neutrons only intensities of primary γ-rays relative to a given transition are given [35]. Therefore, their absolute contribution was varied with a factor ranging from 0.3 to 1.6 and the resulting missing contribution of γ-ray transitions was calculated.

The contribution of transitions with an energy below 330 keV was estimated and the results are summarized in table 3. This was done for *s*- and *p*-wave capture states. For the 4.9 eV *s*-wave resonance about 30.7% of all the transitions are below the 330 keV threshold. When weighting the intensities with the transition energies this missing contribution reduces to 2.48%. The results in table 3 reveal that for all cases the loss in weighted contribution of transitions below 330 keV varies between 2.29% and 2.67%, which is very similar to the corresponding loss for the 4.9 eV resonance. Hence, a bias due to the threshold is expected to be less than 0.5% and the total uncertainty due to the normalization and weighting function was estimated to be less than 1%.

3.4 Time of flight to energy conversion

The time of flight t was derived from the difference between the stop signal T_S and start signal T_0:

$$t = (T_S - T_0) + t_0, \tag{5}$$

where t_0 is a time-offset. This time-offset for the capture detection system was deduced from the position of the γ-ray flash with an accuracy better than 1 ns. The conversion from TOF to energy is also related to the response function of the TOF-spectrometer, which is dominated by the neutron transport in the target/moderator assembly. This response is mostly represented by the distribution of an equivalent distance [11]. A resonance shape analysis of ^{197}Au(n, γ) resonances below 200 eV was used to define the effective flight path length (12.943 ± 0.002 m). The energies of these resonances have been determined by Massimi *et al.* [36,28] from transmission measurements at a 50 m station which was calibrated using the 6.673 ± 0.001 eV resonance of ^{238}U+n as a reference [37]. The final uncertainty on the neutron energy is 0.3%, which was verified using the resonances at 5.904 keV and 71.22 keV of ^{27}Al and ^{208}Pb, respectively.

3.5 Correction for self-shielding and scattering in the sample

In the URR averaged capture cross sections can only be derived by correcting the observed experimental yield for self-shielding and multiple interaction events, *i.e.* neutron scattering followed by neutron capture. The relation between the average capture cross section $\overline{\sigma}_\gamma$ and the average experimental yield $\overline{Y}_{\rm exp}$ is given by

$$\overline{Y}_{\rm exp} = F_c n \overline{\sigma}_\gamma, \tag{6}$$

where F_c is an energy-dependent factor to correct for multiple interaction events and n is the areal density of the sample. The correction factor F_c was calculated by Monte Carlo simulations using SESH [38] and MCNP 4C2 [39]. The former accepts average resonance parameters as input parameters (*i.e.* the average resonance spacing, neutron strength functions and average radiation widths) to create resonance structured cross sections. In MCNP probability tables are used to reconstruct resonance structured cross sections in the URR. These probability tables were

Table 3. Relative intensities of primary γ-ray transitions and transitions with a γ-ray energy smaller than 330 keV for a 4.9 eV, 2 keV and 24 keV incident neutron energy. Both energy weighted and non-weighted intensities are given. For 2 keV and 24 keV neutrons, the intensities are calculated supposing pure s- and p-wave neutrons and different contributions of primary transitions to low-lying excited states (third column).

Neutron energy		Intensity of primary transitions to low-lying excited states relative to all primary transitions	Relative intensity of all primary transitions		Relative intensity of transitions with $E_\gamma < 330$ keV	
			no weight	weighted	no weight	weighted
		%	%	%	%	
4.9 eV	s-wave	16.6	25.0	63.4	30.7	2.48
2 keV	s-wave	9.5	24.8	60.4	26.2	2.25
	p-wave	9.2	23.9	60.3	30.8	2.65
	s-wave	22.9	26.4	65.6	28.3	2.29
	p-wave	22.2	25.4	65.5	32.8	2.66
	s-wave	34.3	28.2	70.3	30.0	2.31
	p-wave	33.5	26.9	70.0	34.8	2.67
24 keV	s-wave	9.1	23.9	60.0	29.6	2.46
	p-wave	8.8	23.7	59.8	30.6	2.63
	s-wave	20.2	25.1	64.5	31.4	2.49
	p-wave	19.9	25.0	64.3	32.4	2.65
	s-wave	29.9	26.3	68.4	33.5	2.55
	p-wave	29.3	26.2	68.1	34.0	2.67

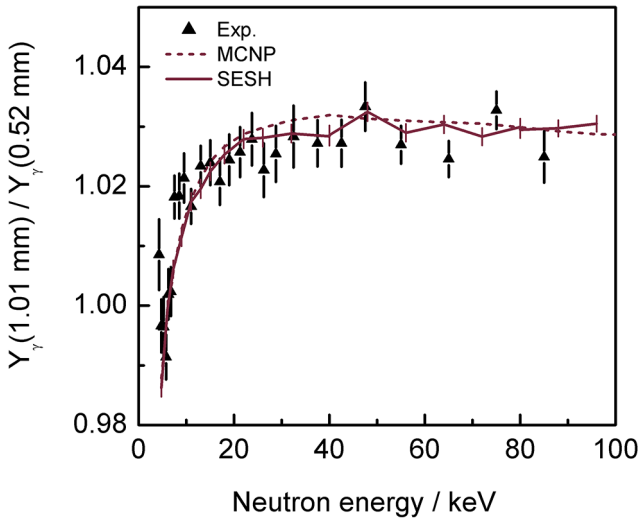

Fig. 4. Ratio of the correction factor F_c for a 1.01 and 0.52 mm thick metal gold sample. The ratio of the experimental yield is compared with the results from calculations with MCNP/NJOY and SESH.

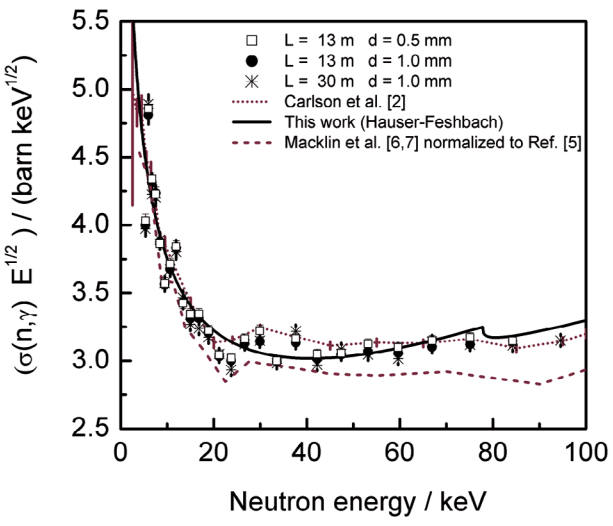

Fig. 5. Average capture cross section for Au(n, γ) as a function of neutron energy in the URR. The cross section obtained in this work is compared with the one recommended in ref. [2] and the one used for astrophysical applications [5]. The cross section derived from the average resonance parameters in table 5 is also shown.

created by NJOY [40]. The average parameters used as input in SESH and NJOY are discussed in sect. 4.2. The theoretical correction factor was verified by comparing the ratio of the experimental yield obtained with the 1.01 mm and 0.52 mm thick sample with the ratio of the calculated correction factors. The results in fig. 4 demonstrate the good agreement between the experimental and calculated results. They also illustrate the consistency between results obtained with MCNP and SESH as already noticed in [11]. From the results in fig. 4 an uncertainty of less than 0.5% on the correction factor F_c was estimated.

Table 4. Average capture cross section ($\overline{\sigma}_\gamma$) and total uncertainty derived from the data obtained in this work. The information to derive the full covariance matrix based on the AGS concept (eq. (7)) is given: the diagonal elements of the uncorrelated components, $u_u = \sqrt{U_u}$ are in column 6, whereas columns 7–10 represent the matrix $S_{\eta=\{b_0,k_1,k_2,N_c\}}$. A high precision is given to ensure that the resulting covariance matrix can be inverted. The correction factor F_c for self-shielding multiple interaction is given in column 3.

E_l/eV	E_h/eV	F_c	$\overline{\sigma}_\gamma$/b	$u_{\overline{\sigma}_\gamma}$/b	AGS				
					u_u/b	S_{b_0}/b	S_{k_1}/b	S_{k_2}/b	S_{N_C}/b
3500	4000	0.9893	2.8696	0.0354	0.0084	−0.001731	−0.012957	−0.004330	0.031566
4000	4500	1.0022	2.2833	0.0284	0.0070	−0.001352	−0.010596	−0.003448	0.025116
4500	5000	1.0113	2.0888	0.0251	0.0058	−0.000981	−0.007942	−0.002375	0.022977
5000	5500	1.0180	1.5480	0.0190	0.0047	−0.000803	−0.006683	−0.001828	0.017028
5500	6000	1.0232	2.1886	0.0259	0.0057	−0.000734	−0.006767	−0.003384	0.024075
6000	6500	1.0273	1.7350	0.0207	0.0051	−0.000649	−0.006058	−0.001689	0.019085
6500	7000	1.0306	1.7219	0.0204	0.0049	−0.000567	−0.005428	−0.001737	0.018941
7000	8000	1.0345	1.5664	0.0184	0.0036	−0.000554	−0.005162	−0.001519	0.017230
8000	9000	1.0385	1.3120	0.0156	0.0034	−0.000494	−0.004555	−0.001419	0.014432
9000	10000	1.0414	1.1502	0.0137	0.0032	−0.000437	−0.004116	−0.001166	0.012652
10000	12000	1.0446	1.1625	0.0135	0.0023	−0.000374	−0.003588	−0.001109	0.012788
12000	14000	1.0475	0.9572	0.0113	0.0022	−0.000324	−0.003234	−0.000963	0.010529
14000	16000	1.0495	0.8569	0.0102	0.0022	−0.000283	−0.002963	−0.000830	0.009426
16000	18000	1.0509	0.8215	0.0097	0.0022	−0.000250	−0.002674	−0.000756	0.009037
18000	20000	1.0519	0.7329	0.0087	0.0021	−0.000225	−0.002411	−0.000705	0.008062
20000	24000	1.0529	0.6418	0.0076	0.0015	−0.000195	−0.002145	−0.000650	0.007060
24000	28000	1.0538	0.6165	0.0072	0.0015	−0.000168	−0.001929	−0.000703	0.006781
28000	32000	1.0542	0.5842	0.0076	0.0026	−0.000242	−0.002914	−0.000896	0.006426
32000	36000	1.0544	0.5160	0.0062	0.0016	−0.000144	−0.001835	−0.000669	0.005676
36000	40000	1.0544	0.5168	0.0061	0.0015	−0.000122	−0.001581	−0.000575	0.005685
40000	44000	1.0543	0.4709	0.0056	0.0014	−0.000103	−0.001343	−0.000487	0.005180
44000	52000	1.0539	0.4403	0.0051	0.0010	−0.000089	−0.001119	−0.000440	0.004843
52000	60000	1.0533	0.4192	0.0049	0.0011	−0.000088	−0.001074	−0.000610	0.004612
60000	68000	1.0526	0.3894	0.0045	0.0009	−0.000062	−0.000739	−0.000523	0.004284
68000	76000	1.0517	0.3771	0.0043	0.0009	−0.000054	−0.000632	−0.000500	0.004148
76000	84000	1.0508	0.3429	0.0039	0.0009	−0.000054	−0.000619	−0.000335	0.003772

4 Results

4.1 Experimental average capture in the unresolved resonance region

The experimental average capture cross section derived from the data obtained in this work is plotted as a function of neutron energy in fig. 5. The results are compared with the cross section resulting from the standards evaluation [2] and the one recommended for astrophysical applications [5]. This figure demonstrates that the average capture cross section obtained in this work is in good agreement with the standard evaluation. On average the results of the standards evaluation are about 1.5% higher. This difference is much smaller compared to the difference with the one recommended for astrophysical applications, which is on average about 6%. However, the data obtained in this work show fluctuations which are not present in the cross section recommended in refs. [1,2]. To verify the origin of these fluctuations, additional capture measure-

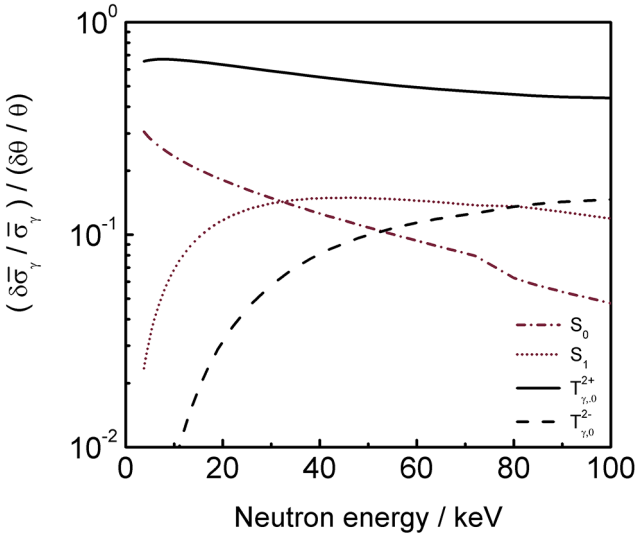

Fig. 6. Sensitivity $(\delta\overline{\sigma}_\gamma/\overline{\sigma}_\gamma)/\ (\delta\theta/\theta)$ of the average capture cross section to the average parameter θ as a function of neutron energy. The parameter θ represents either the neutron strength functions $S_{\ell=0,1}$ or γ-ray transmission coefficients $T^{2^+}_{\gamma,0}$ and $T^{2^-}_{\gamma,0}$.

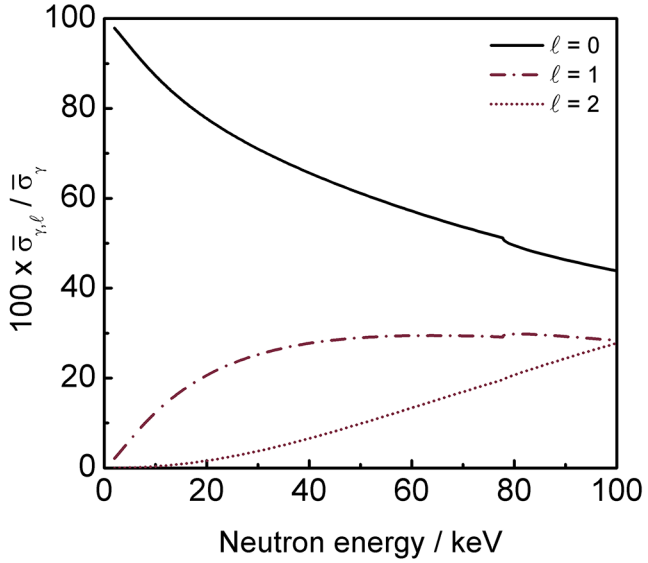

Fig. 7. Relative contribution of s-, p- and d-wave neutrons ($\ell = 0, 1$ and 2) to the average capture cross section $\overline{\sigma}_\gamma$ for ^{197}Au(n, γ) as a function of neutron energy.

ments at a 30 m station with the 1.01 mm thick sample were performed. Since the experiments were carried out with the accelerator operating at 800 Hz, an absolute normalization based on the 4.9 eV saturated resonance was not possible. Hence, the results from the 30 m measurements can only be used as relative data. The results in fig. 5 confirm the fluctuations observed in the data obtained at the 13 m flight path and suggest that they are due to clusters of resonances. Below 20 keV the cross section derived by Lederer *et al.* [10] from measurements at the n_TOF facility shows similar structures.

The average capture cross sections between 3.5 keV and 84 keV derived from the data described in this work, together with a full covariance information using the AGS concept [25] are given in table 4. In this table the total uncertainty and uncertainty due to uncorrelated components are separately given. Applying the AGS concept described in ref. [25] the covariance matrix $\mathsf{V}_{\overline{\sigma}_\gamma}$ of the experimental average capture cross section is given by

$$\mathsf{V}_{\overline{\sigma}_\gamma} = \mathsf{U}_u + \mathsf{S}(\eta)\mathsf{S}^T(\eta), \tag{7}$$

where U_u is a diagonal matrix containing the contribution of all uncorrelated uncertainty components and $\mathsf{S}(\eta)$ is a matrix representing the correlated contribution of components $\eta = \{b_0, k_1, k_2, N_c\}$, creating a correlated contribution. Hence, the data in table 4 can be used to calculate the full covariance and verify the impact of the uncertainty due to N_C, k_1 and k_2. The contribution of other effects such as the areal density of the sample, dead time correction and background on the flux measurements can be neglected.

Table 5. Average parameters (R', $S_{\ell=0,1}$, $T^{2^+}_{\gamma,0}$, $T^{2^-}_{\gamma,0}$) and their covariance matrix derived from a least-squares adjustment to the experimental average capture cross section and the average total cross section of refs. [47–49].

	θ	u_θ	Correlation matrix ×1000				
R'/fm	9.193	0.056	1000	−401	−239	141	33
$S_0/10^{-4}$	1.947	0.027	−401	1000	512	−324	−13
$S_1/10^{-5}$	2.836	0.077	−239	512	1000	−398	−607
$T^{2^+}_{\gamma,0}/10^{-2}$	3.441	0.062	141	−324	−398	1000	740
$T^{2^-}_{\gamma,0}/10^{-2}$	1.622	0.062	33	−13	−607	740	1000

4.2 Parameterization of the ^{197}Au(n, γ) cross section in the unresolved resonance region

In the URR average compound cross sections can be parameterized in terms of transmission coefficients by means of the Hauser-Feshbach statistical reaction theory with width - fluctuations, following various schemes for the fluctuation correction factor [41–44]. The width fluctuation correction factor approach used in this work has been the ENDF statistical integration with a Gauss quadrature scheme [45] which is equivalent to an accurately calculated Dresner integral and compatible with the ENDF-6 format/model. In the absence of direct reactions, the average capture cross section depends on the neutron strength functions and the capture transmission coefficients. In most cases the neutron strength functions can be considered as being energy independent. The energy dependence of the transmission coefficient for the capture channel $T^{J^\pi}_\gamma$ can be parameterized by [46]

$$T^{J^\pi}_\gamma(E) = T^{J^\pi}_{\gamma,0} W_{T^{J^\pi}_\gamma}(E), \tag{8}$$

Table 6. Average total and capture cross sections together with their covariance data derived from the parameters given in table 5.

E/eV	$\sigma_{\rm tot}$/b	$u_{\rm tot}$/b	Correlation matrix ×1000									
5000	21.08	0.14	1000	958	802	666	582	36	21	31	31	6
10000	17.56	0.12	958	1000	940	852	791	23	14	20	20	5
25000	14.20	0.10	802	940	1000	980	952	4	3	3	3	2
50000	12.28	0.10	666	852	980	1000	994	−9	−5	−8	−8	−2
80000	11.19	0.09	582	791	952	994	1000	−17	−10	−14	−14	−5
	σ_γ/b	u_γ/b										
5000	2.040	0.023	36	23	4	−9	−17	1000	998	991	989	983
10000	1.186	0.013	21	14	3	−5	−10	998	1000	997	992	982
25000	0.624	0.007	31	20	3	−8	−14	991	997	1000	995	981
50000	0.430	0.005	31	20	3	−8	−14	989	992	995	1000	994
80000	0.355	0.004	6	5	2	−2	−5	983	982	981	994	1000

where $T_{\gamma,0}^{J^\pi} = T_\gamma^{J^\pi}(E=0)$ is the capture transmission coefficient at zero neutron energy. The energy dependence $W_{T\gamma}^{J^\pi}(E)$ is determined from the $T_\gamma^{J^\pi}(E)$ definition as a sum of single-channel photon transmission coefficients. The summation (integration) is over the transition types, multipolarities and photon energies of the primary gamma rays that deexcite the compound nucleus to lower-lying states of a given density. The J dependence of $T_\gamma^{J^\pi}$ is usually determined from the J dependence of the level density with the common assumption that the effective radiation widths only depend on the parity. Hence, independent parameters to determine the average capture cross section in the URR are the neutron strength functions S_ℓ and the capture transmission coefficients $T_{\gamma,0}^{J^\pi}$ that belong to different parities (even and odd ℓ), *e.g.* $T_{\gamma,0}^{(I+1/2)^+}$ and $T_{\gamma,0}^{(I+1/2)^-}$, where I is the target spin.

The sensitivity of the average capture cross section for ^{197}Au to the strength functions $S_{\ell=0,1}$ and to the capture transmission coefficients $T_{\gamma,0}^{2^+}$ and $T_{\gamma,0}^{2^-}$ is shown in fig. 6 as a function of neutron energy. This figure reveals that the capture cross section for ^{197}Au in the energy region between 4 keV and 100 keV is mainly sensitive to $T_{\gamma,0}^{2^+}$. The low sensitivity to the p- and d-wave parameters follows also from fig. 7 which gives the relative contribution of the partial waves to the average capture cross section.

Average parameters, *i.e.* an orbital independent scattering radius, strength functions $S_{\ell=0,1}$ and capture transmission coefficients for s-waves $T_{\gamma,0}^{2^+}$ and p-waves $T_{\gamma,0}^{2^-}$ were derived from a least squares adjustment to the experimental average cross section discussed in sect. 4.1 together with the average total cross section of Poenitz *et al.* [47] and Purtov *et al.* [48] and results from TOF transmission measurements at the GELINA facility reported by Sirakov *et al.* [49]. The generalized ENDF-6 model together with the standard boundary conditions has been used (see Sirakov *et al.* [49]). The capture channel transmission coefficients for d-wave neutrons have been determined from the s-wave coefficient. The strength function for d-waves S_2 was taken from ref. [50]. In the calculations the correlated and uncorrelated components reported by Poenitz *et al.* [47] and Sirakov *et al.* [49] were taken into account. In the paper of Purtov *et al.* [48] the different uncertainty components are not discussed. For these data a 2% normalization uncertainty was included. To avoid bias effects due to Peelle's Pertinent Puzzle [51], the uncertainties due to the normalization of the capture data and the data of refs. [47,48] were based on the parameterized cross section [52]. The resulting parameters with the covariance matrix are listed in table 5 and the capture cross section calculated with these parameters is shown in fig. 5. The calculated total and capture cross sections together with the covariance matrix are reported in table 6.

4.3 Maxwellian average capture cross section for ^{197}Au(n, γ)

Given the importance of Maxwellian Average Cross Sections (or MACS) for astrophysical applications and for cross section measurements based on neutron activation combined with accelerator mass spectrometry [53], MACS for the ^{197}Au(n, γ) reaction at different temperatures were studied. To verify the impact of the resonance fluctuations in the capture cross section, MACS were calculated based on both the cross section derived directly from the experimental data (table 4) and the parameterized cross section using the parameters in table 5. For energies outside the range covered in table 4 (*i.e.* energies below 3.5 keV and above 84 keV) the capture cross section of JEFF-3.2 [50] was adopted. The capture cross section for energies above 2 keV in JEFF-3.2 was taken from Carlson *et al.* [2]. The results are summarized in table 7. The uncertainties on the MACS derived from the data reported in this work are dominated by the 1.0% uncertainty on the normalization. In this table MACS based on JEFF-3.2 and from the KADoNiS v03 [54] library used for astrophysical calculations are also given. The results in table 7 show that the difference between the MACS derived from the experimental and calculated cross section is maximum 0.5%. Hence, the impact of the resonance fluctuations between 3.5 keV

Table 7. Maxwellian averaged capture cross sections (MACS) at different temperatures. The MACS derived from the experimental data in table 4 and from the calculated cross section using the parameters in table 5 are compared with the ones derived from the cross section in JEFF-3.2 [50] and with the ones from the KADoNiS v03 library [54].

kT/keV	MACS/mb			
	Experimental	Calculated	JEFF-3.2	KADoNis v0.3
5	2124.3	2113.2	2132.8	2050
10	1257.7	1253.7	1272.3	1208
15	944.9	941.8	956.9	904
20	783.3	780.5	792.3	746
25	684.0	681.6	690.7	648
30	613.3	611.3	618.4	582
40	522.9	521.5	526.1	496
50	462.5	461.5	464.7	442

and 84 keV is very small. The maximum deviation between the MACS derived from the cross section obtained in this work and the one in JEFF-3.2, which includes the one of Carlson *et al.* [2], is 1.5%. The MACS derived in this work are systematically about 5% higher compared to those in the KADoNiS v03 [54] library.

5 Conclusions

Measurements have been performed at the GELINA facility to determine the average cross section for the ^{197}Au(n, γ) reaction in the 3.5 keV to 84 keV energy region. Using an internal normalization procedure, the systematic uncertainty related to the normalization and weighting function is less than 1%. The uncertainty due to self-shielding and multiple scattering corrections is less than 0.5%. A full covariance matrix has been produced by propagating both uncorrelated and correlated uncertainties. Fluctuations due to resonance structure were verified by measurements at different flight path lengths.

Average resonance parameters, *i.e.* an orbital independent scattering radius R', strength functions $S_{\ell=0,1}$ and capture transmission coefficients for s-waves $T^{2^+}_{\gamma,0}$ and p-waves $T^{2^-}_{\gamma,0}$, together with their covariance matrix have been derived in a simultaneous least squares fit to the average capture cross section obtained in this work and experimental average total cross sections reported in the literature.

The data reported in this work are on average 6% higher than the cross sections adopted for astrophysical applications. However, they are about 1.5% lower compared to a recommended cross section which resulted from a least squares analysis of experimental data that was available in the literature prior to this work. Given the uncertainty reached in the present experiment, the results in this work confirm the bias in the cross sections used for astrophysical applications.

We are grateful to the GELINA operators for the dedicated and skillful running of the accelerator as well as to the Nuclear Energy Agency of the OECD and the Nuclear Data Section of the IAEA for their interest in the present research. This work was partly supported by the European Commission through the projects EFNUDAT (FP6-036434) and ERINDA (FP7-269499). We also acknowledge the work of the anonymous referees for their valuable comments and suggestions which improved the original manuscript.

References

1. S.A. Badikov, Chen Zhenpeng, A.D. Carlson, E.V. Gai, G.M. Hale, F.-J. Hambsch, H.M. Hofmann, T. Kawano, N.M. Larson, V.G. Pronyaev, D.L. Smith, Soo-Youl Oh, S. Tagesen, H. Vonach, IAEA Report, STI/PUB/1291 (2007).
2. A.D. Carlson, V.G. Pronyaev, D.L. Smith, N.M. Larson, Z. Chen, G.M. Hale, F.-J. Hambsch, E.V. Gai, Soo-Youl Oh, S.A. Badikov, T. Kawano, H.M. Hofman, H. Vonach, S. Tagesen, Nucl. Data Sheets **110**, 3215 (2009).
3. A.D. Carlson, V.G. Pronyaev, F.-J. Hambsch, F. Käppeler, W. Mannhart, A. Mengoni, R.O. Nelson, P. Talou, S. Tagesen, H. Vonach, J. Kor. Phys. Soc. **59**, 1390 (2011).
4. W.P. Poenitz, *Data Interpretation, Objective, Evaluation Procedures and Mathematical Technique for the Evaluation of Energy-Dependent Ratio, Shape and Cross Section Data*, in *Proceedings of the Conference on Nuclear Data Evaluation Methods and Procedures*, BNL-NCS-51363, Vol. **2** (1981) p. 249.
5. W. Ratynski, F. Käppeler, Phys. Rev. C **37**, 595 (1988).
6. R.L. Macklin, J. Halperin, R.R. Winters, Phys. Rev. C **11**, 1270 (1975).

7. R.L. Macklin, Nucl. Sci. Eng. **79**, 265 (1981).
8. A. Borella, K. Volev, A. Brusegan, P. Schillebeeckx, F. Corvi, N. Koyumdjieva, N. Janeva, A.A. Lukyanov, Nucl. Sci. Eng. **152**, 1 (2006).
9. G. Feinberg, M. Friedman, A. Kràsa, A. Shor, Y. Eisen, D. Berkovits, D. Cohen, G. Giorginis, T. Hirsh, M. Paul, A.J.M. Plompen, E. Tsuk, Phys. Rev. C **85**, 055810 (2012).
10. C. Lederer *et al.*, Phys. Rev. C **83**, 034608 (2011).
11. P. Schillebeeckx, B. Becker, Y. Danon, K. Guber, H. Harada, J. Heyse, A.R. Junghans, S. Kopecky, C. Massimi, M. Moxon, N. Otuka, I. Sirakov, K. Volev, Nucl. Data Sheets **113**, 3054 (2012).
12. N. Yamamuro, T. Hayase, T. Doi, Y. Fujita, K. Kobayashi, R.C. Block, Nucl. Instrum. Methods **133**, 531 (1976).
13. W. Mondelaers, P. Schillebeeckx, Notizario **11**, 19 (2006).
14. D. Tronc, J.M. Salomé, K.H. Böckhoff, Nucl. Instrum. Methods A **228**, 217 (1985).
15. J.M. Salome, R. Cools, Nucl. Instrum. Methods **179**, 13 (1981).
16. R.L. Macklin, J.H. Gibbons, Phys. Rev. **159**, 1007 (1967).
17. A. Borella, G. Aerts, F. Gunsing, M. Moxon, P. Schillebeeckx, R. Wynants, Nucl. Instrum. Methods A **577**, 626 (2007).
18. P. Schillebeeckx, A. Borella, S. Kopecky, C. Lampoudis, C. Massimi, M. Moxon, J. Kor. Phys. Soc. **59**, 1563 (2011).
19. S. de Jonge, *Fast Time Digitizer Type 8514 A*, Internal Report GE/DE/R/24/87, IRMM, Geel (1987).
20. J. Gonzalez, C. Bastian, S. de Jonge, K. Hofmans, *Modular Multi-Parameter Multiplexer MMPM. Hardware description and user guide*, Internal Report GE/R/INF/06/97, IRMM, Geel (1997).
21. L.C. Mihailescu, A. Borella, C. Massimi, P. Schillebeeckx, Nucl. Instrum. Methods A **600**, 453 (2009).
22. `http://www.mitutoyo.com/`.
23. G. Giorginis, V. Khriatchkov, Nucl. Instrum. Methods A **538**, 550 (2005).
24. C. Bastian, *General procedures and computational methods for generating covariance matrices*, in *Proc. Int. Symp. on Nuclear Data Evaluation Methodology* (1992) p. 642.
25. B. Becker, C. Bastian, F. Emiliani, F. Gunsing, J. Heyse, K. Kauwenberghs, S. Kopecky, C. Lampoudis, C. Massimi, N. Otuka, P. Schillebeeckx, I. Sirakov, JINST **7**, P11002 (2012).
26. N. Otuka, A. Borella, S. Kopecky, C. Lampoudis, P. Schillebeeckx, J. Kor. Phys. Soc. **59**, 1314 (2011).
27. M.C. Moxon, J.B. Brisland, *GEEL REFIT, A least squares fitting program for resonance analysis of neutron transmission and capture data computer code*, in AEA-InTec-0630, AEA Technology, October 1991.
28. C. Massimi, A. Borella, S. Kopecky, C. Lampoudis, P. Schillebeeckx, M.C. Moxon, G. Vannini, J. Kor. Phys. Soc. **59**, 1689 (2011).
29. G. Schramm, R. Massarczyk, A.R. Junghans *et al.*, Phys. Rev. C **85**, 014311 (2012).
30. R. Massarczyk, G. Schramm, A.R. Junghans, R. Schwengner, M. Anders, T. Belgya, R. Beyer, E. Birgersson, A. Ferrari, E. Grosse, R. Hannaske, Z. Kis, T. Kögler, K. Kosev, M. Marta, L. Szentmiklósi, A. Wagner, J.L. Weil, Phys. Rev. C **87**, 044306 (2013).
31. F. Bečvář, Nucl. Instrum. Methods A **417**, 434 (1998).
32. A.R. Junghans, G. Rusev, R. Schwengner, A. Wagner, E. Grosse, Phys. Lett. B **670**, 200 (2008).
33. K. Heyde, P. von Neumann-Cosel, A. Richter, Rev. Mod. Phys. **82**, 2365 (2010).
34. R. Capote, M. Herman, P. Obložinský, P.G. Young, S. Goriely, T. Belgya, A.V. Ignatyuk, A.J. Koning, S. Hilaire, V.A. Plujko, M. Avrigeanu, O. Bersillon, M.B. Chadwick, T. Fukahori, Zhigang Ge, Yinlu Han, S. Kailas, J. Kopecky, V.M. Maslov, G. Reffo, M. Sin, E.Sh. Soukhovitskii, P. Talou, Nucl. Data Sheets **110**, 3107 (2009).
35. Huang Xiaolong, Nuclear Data Sheets **110**, 2533 (2009).
36. C. Massimi, A. Borella, S. Kopecky, C. Lampoudis, M. Moxon, P. Schillebeeckx, G. Vannini, Nuovo Cimento B **125**, 517 (2010).
37. H. Derrien, L.C. Leal, N.M. Larson, A. Courcelle, *Neutron Resonance Parameters and Calculated Cross Sections from Reich-Moore Analysis of Experimental Data in the Neutron Energy Range from* 0 *to* 20 keV, in ORNL/TM-2005/241, Oak Ridge National Laboratory (2005).
38. F. Fröhner, *SESH A Fortran IV code for calculating the self-shielding and multiple scattering effects for neutron cross section data interpretation in the unresolved resonance region*, in Report GA-8380, Gulf General Atomic (1968).
39. J. Briemeister, *MCNP, A General Monte Carlo N-Particle Transport Code, Version 4C2*, in LA-13709-M (2000).
40. R.E. MacFarlane, A.C. Kahler, Nucl. Data Sheets **111**, 2739 (2010).
41. L. Dresner, *Proceedings of the International Conference on Neutron Reactions with the Nucleus, Columbia Univ., 1957*, Report CU-157 (1957) p. 71.
42. P.A. Moldauer, Nuclear Physics A **344**, 185 (1980).
43. H.M. Hofman, J. Richert, J.W. Tepel, W.A. Weidenmuller, Nucl. Phys. A **344**, 402 (1975).
44. J.J.M. Verbaarschot, H.A. Weidenmüller, M.R. Zirnbauer, Phys. Rep. **129**, 367 (1985).
45. H. Henryson, B.J. Toppel, C.G. Sternberg, Argonne National Laboratory Report ANL-8144 (ENDF-239) (1976).
46. I. Sirakov, R. Capote, F. Gunsing, P. Schillebeeckx, A. Trkov, Ann. Nucl. Energy **35**, 1223 (2008).
47. W.P. Poenitz, J.F. Whalen, A.B. Smith, Nucl. Sci. Eng. **78**, 333 (1981).
48. O.A. Purtov, L.L. Litvinskiy, A.V. Murzin, G.M. Novoselov, At. Energy **77**, 536 (1994).
49. I. Sirakov, B. Becker, R. Capote, E. Dupont, S. Kopecky, C. Massimi, P. Schillebeeckx, Eur. Phys. J. A **49**, 144 (2013).
50. I. Sirakov, B. Becker, R. Capote, S. Kopecky, C. Massimi, V. Pronayev, P. Schillebeeckx, A. Trkov, G. Žerovnik, Evaluation of Neutron Induced Reaction Cross Sections on Gold, JRC Scientific and Policy Report, EUR 25803 EN (2013).
51. G. D'Agostini, Nucl. Instrum. Methods A **346**, 306 (1994).
52. B. Becker, R. Capote, S. Kopecky, C. Massimi, P. Schillebeeckx, I. Sirakov, K. Volev, Nucl. Data Sheets **118**, 381 (2014).
53. A. Wallner, K. Buczak, F. Quinto, P. Steier, T. Belgya, L. Szentmiklosi, M. Bichler, I. Dillmann, F. Käppeler, A. Mengoni, J. Kor. Phys. Soc. **59**, 1410 (2011).
54. I. Dillmann, R. Plag, F. Käppeler, T. Rauscher, *KADoNiS v0.3 - The third update of the "Karlsruhe Astrophysical Database of Nucleosynthesis in Stars"*, in *Proc. of the EFNUDAT Fast Neutrons Workshop, 28, 30 April, 2009, Geel, Belgium* (2010) p. 55.